First publ. in: Review of Scientific Instruments 79 (2008), 093901

Nanofabricated adjustable multicontact devices on membranes

Reimar Waitz,[1] Olivier Schecker,[1,2] and Elke Scheer[1]
[1]Department of Physics, University of Konstanz, D-78457 Konstanz, Germany
[2]IMEP-LAHC, MINATEC-INPG, F-38016 Grenoble, France

(Received 2 June 2008; accepted 25 July 2008; published online 8 September 2008)

Adjustable atomic size contacts realized by break junctions have become a standard tool during the last decade. Although nanofabricated break junctions may in principle be incorporated onto complex electronic circuits, a fundamental drawback of the standard break junction technique is its limitation to a single adjustable junction per device. We have fabricated single break junctions as well as devices containing two break junctions on a silicon membrane. The junctions are adjusted by positioning a fine tip via piezocontrol on the rear side of the membrane. We describe the fabrication process of the membranes and the devices and present results obtained on circuits made of gold and platinum. We show that the junctions can be addressed independently by a suitable choice of the tip position. Single-atom contacts, vacuum tunneling contacts as well as larger contacts can be stabilized.

I. INTRODUCTION

The investigation of electrical properties of matter at the atomic level has become possible by the development of techniques such as the scanning tunneling microscope or mechanically controllable break junctions (MCBs).[1] A variety of realizations of MCBs have been put forward including "notched-wire" MCBs (Ref. 2) and lithographically defined MCBs.[3] So far they have in common a bulk substrate made of metal, plastic, or silicon. The adjustment is performed by uniformly bending the substrate. A pushing rod is placed at the rear side of the device closely to the single break junction and two countersupports insure the bending. Since the typical dimension of the bending mechanism is on the millimeter to centimeter scale, it is impossible to integrate and address in a controllable way more than one junction.

We have overcome this restriction by defining MCBs on silicon membranes produced from silicon-on-insulator (SOI) wafers.[4] We use the elasticity of the membranes to expand them locally with the help of a thin tip and by this means to stretch the metallic nanostructures on top. By displacing the tip in the plane of the membrane the point of maximum expansion can be adjusted according to the designed device. The lateral positioning precision is in the order of micrometers.

In standard MCB realizations the junctions are suspended from the substrate by several hundred nanometers to micrometers.[3] This is advantageous to exclude possible influence from the substrate, e.g., in molecular electronics applications.[5] However, it hampers using the substrate as back gate or for imaging field distributions.[6,7] On bulky substrates the high suspension is necessary to ensure reliable breaking of the contacts because a particular freestanding length is required for breaking the junctions by elastic and reversible deformation of the substrate. As a compromise a combination of lithographically defined MCBs with electromigration for reducing the initial thickness of the nanobridge has been put forward.[8] Since in our new device the quantity which defines the elongation of the metal structures is the strain and the elastic expansion resulting from the strain, the suspension height may be reduced considerably without further reduction of the lithographically defined bridge diameter [see Figs. 1(a) and 2].

II. SAMPLE FABRICATION PROCEDURE

We start from SOI wafers (Company SOITEC, Grenoble) into which we define freestanding single-crystalline membranes out of Si with a thickness of 340 ± 5 nm, which is defined by the thickness of the silicon top layer by the fabrication process of the wafer. The crystal orientation of the membrane is [100]. The top layer resides on an oxide layer produced by thermal oxidation of Si with an approximate thickness of 400 ± 15 nm. Smaller Si thicknesses down to 24 nm (Ref. 10) have been reported in literature. Our fabrication process is similar to the one described in Ref. 9. After having produced the membranes with a size of 0.6×0.6 mm^2, we cover the wafers with the membranes with a 100 nm thin layer of polyimide (T-10001 from Brewer Science Inc.) using an adhesion promoter APX-K1 from the same company. This layer has a twofold function. At first it can be etched away in order to suspend the metallic nanobridges and secondly it isolates the metallic nanostructures electrically from the silicon substrate which has a finite conductance at room temperature (ρ ranges from 14 to 22 Ω cm). We then cover the substrates with a standard double layer system of polymethyl methacrylate (PMMA, 100 nm thick) and methyl methacrylate-methacrylic acid (MMA-MAA, 600 nm thick) for electron beam lithography and cut the wafer in quadratic pieces of 8×8 mm^2. We perform the exposure in a scanning electron microscope equipped with a pattern generator with the desired design. Examples are shown in Figs. 1(a) and 1(b). After development, the metal is evaporated (we tested Al, Pt, and Au) onto the substrate from an electron gun. The next steps are the lift-off of the mask in acetone and isotropic reactive ion etch-

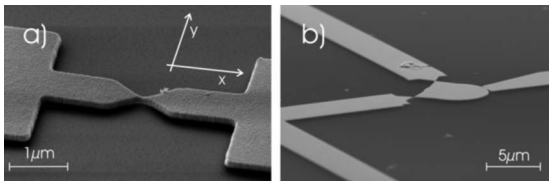

FIG. 1. (a) Electron micrograph of a single gold break junction on a membrane. (b) Electron micrograph of a double junction separated by a circular island of size of 6 μm. For measuring the conductance of both junctions independently a reference electrode has been attached to the island.

ing of the polyimide in oxygen plasma. The goal of this etching step is twofold. First the narrow bridge has to be detached from the substrate in order to guarantee concentration of the mechanical strain at the bridge for reliable breaking. Secondly, the polyimide on the parts of the membrane which are not covered by metal has to be removed for improving the optical and mechanical properties of the membrane. These two requirements can be fulfilled by suitable choice of the etching parameters [pressure of 1 mbar, power of 50 W, flow of 50 SCCM (SCCM denotes cubic centimeter per minute at STP) O_2], which result in an etching rate of 2.5 nm/min laterally. The process is stopped when the metal structures are underetched laterally by $\Delta w \approx 500$ nm. Manifold geometries including single break junctions [Fig. 1(a)] as well as double junctions with a small island in between [Fig. 1(b)] can be fabricated. The minimum island size is limited by the underetching width $D_{\min} > 2\ \Delta w$.

III. MECHANICAL CONTROL SYSTEM

The chips with the membranes are then clamped onto a stretching mechanism consisting of a sample holder which carries the chip and a fine tip controlled by a uniaxial piezostage (from Attocube, model ANPz 100, for the z-motion perpendicular to the membrane), which is itself mounted on a mechanically controlled x-y table [see Fig. 2, for the definition of the x and y directions see Fig. 1(a)]. We use the slip-stick mode of the stage for coarse approach and the piezoeffect of the stage element for the fine adjustment. The resolution of the z-detection of our profilometer is limited to a few nanometers, although the stability of the stage should allow subnanometer precision and the results of our transport measurements also suggest the stability to be in this range

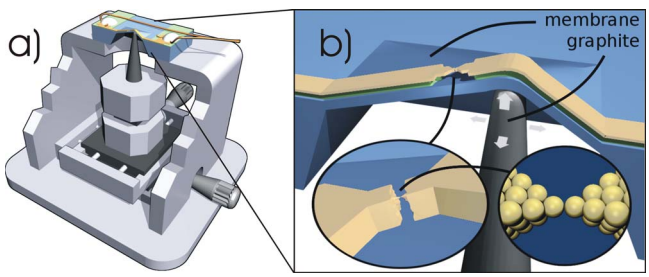

FIG. 2. (Color online) (a) Schematics of the breaking mechanism, showing the sample holder and a cut through a sample (not to scale), the tip, and its control scheme with mechanical x-y stage and piezocontrol for the z motion. (b) Zoom into panel (a) demonstrating the working principle of the setup. The typical membrane size is 0.6×0.6 mm^2 with a thickness of 340 nm.

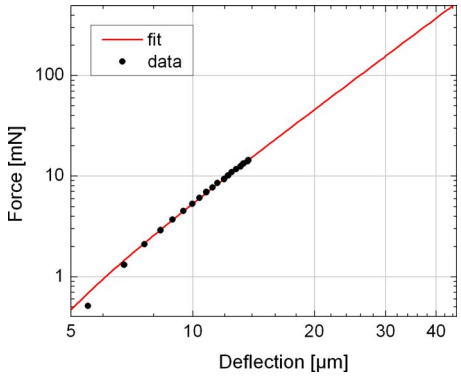

FIG. 3. (Color online) The force needed to cause a given deflection of a membrane with 0.4 mm diameter by applying underpressure on one side. The fit has been performed according to $F(z) = C \times (z^3 - z_0^2 z)$.

(see below). The motion of the tip can be monitored with an optical profiler with integrated microscope and recorded by a charge coupled device camera. The precision with which the tip can be positioned laterally is in the order of 1 μm, given by the precision of the micrometer screws. Upon pushing the tip toward the membrane it is stretched locally. We tried different tip materials including glass, graphite, Macor® ceramics, epoxy, and metal pins. Best results were obtained with glass and graphite. The glass tips have almost spherical ends and are made from short pieces of homemade glass rod with a diameter between roughly 40 and 100 μm by melting the ends and cleaning in ethanol after cooling down. The resulting ends have diameters between 60 and 250 μm. The glass tips are robust and give very reproducible deformations. They are used for the optical measurements described below. However, for experiments which require displacing the tip along the membrane, graphite tips are advantageous, since the glass tips have the tendency to adhere to the membrane and to move laterally in a slip-stick motion. The graphite tips are made from pencils by careful polishing. The effective curvature varies from tip to tip, but is estimated to be in the order of 10–20 μm. While the graphite tips slide easily along the rear side of the membrane, their tip shape changes resulting in strong variations of the required vertical displacement in order to produce a particular deformation of the membrane and in the formation of multiple tips.

The force, which is required to deform the membrane, can be estimated from the deflection of the membrane when expanded by hydrostatic pressure and recording the shape with the profilometer. Since our setup has only the ability to apply underpressure on one side, we are limited to forces lower than 1 atm times the area of the membrane. The fit function we use in Fig. 3 is $F(z) = C \times (z^3 - z_0^2 z)$ with the fit parameters $C = 5.87 \times 10^{-6}$ N/μm^3 and $z_0 = 3.0$ μm. This value of z_0 is in the order of magnitude of the deflection of the membrane without applied pressure. Geometrical considerations lead to a strain proportional to z^2, thus with Hooke's law one expects the energy to increase proportional to z^4 and the force with z^3. This fit function is commonly used in the membrane bulging method for characterizing the elastic properties.[11] Our breaking mechanism usually works at deflections of about 15 μm corresponding to about 20 mN. At forces in the range of 250–500 mN (estimated from that fit)

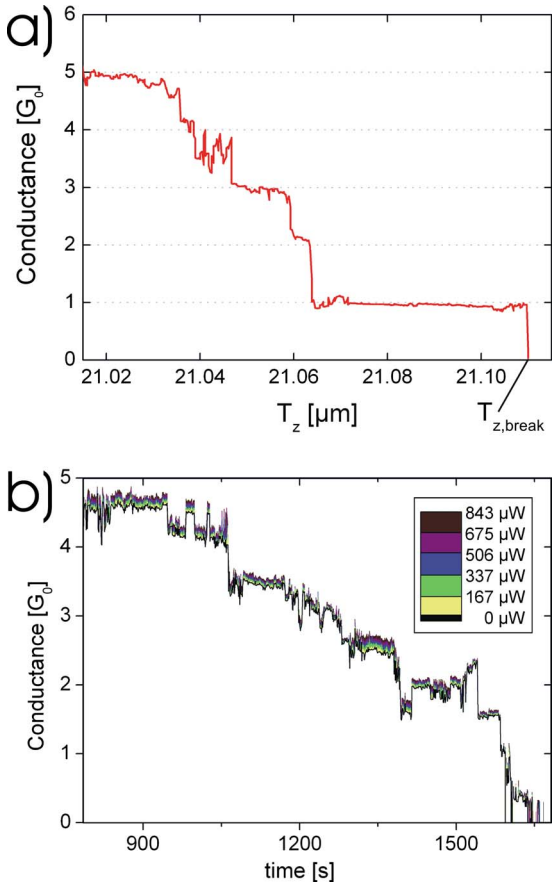

FIG. 4. (Color online) (a) Conductance G as a function of vertical displacement T_z of a gold break junction measured under ambient conditions. (b) Conductance vs time of a gold junction when opened with a constant z-speed of the tip of approximately 1 nm/s and when irradiated with laser light with wavelength $\lambda = 488$ nm and power P as indicated in the legend. The spot has a diameter of approximately 10 μm.

the membranes tend to break. Of course these numbers only represent a rough estimation because with applied pressure, the force is spread over the whole membrane, in contrast to a very concentrated force, which we use for controlling the MCBs.

IV. RESULTS

A. Function and stability of the setup

The operation of the setup is tested by recording the conductance G of a gold break junction as a function of the z-position of the tip T_z. In Fig. 4(a) we show an example of such an "opening trace" when the tip is displaced by 27 μm in x direction from the bridge. The conductance decreases in steps of a typical height of the conductance quantum $G_0 = 2\,e^2/h$ (e: elementary charge; h: Planck's constant). A last step of $G \approx 1G_0$ is observed, which is typical for single-atom contacts of gold.[1] Upon further deformation the metallic contact breaks and a tunneling contact is formed ($T_z = T_{z,\mathrm{break}}$). When the tip is withdrawn the junction closes again to roughly its initial conductance of typically $200G_0$. In order to demonstrate the sensitivity to the lateral position of the tip, we plot in Fig. 5 the displacement in z-direction which is required for breaking a junction to the tunneling regime $T_{z,\mathrm{break}}$ as a function of tip position in x and y direc-

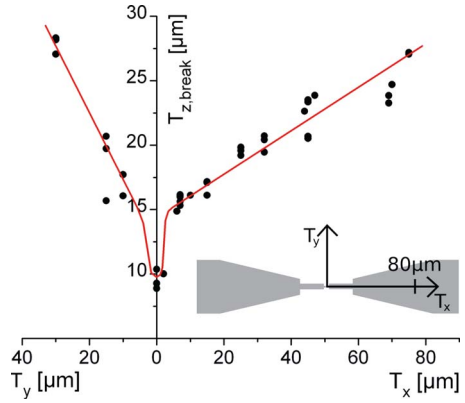

FIG. 5. (Color online) Sensitivity of the setup to lateral motion of the tip. The main panel shows the displacement in z-direction which is required for breaking a nanobridge $T_{z,\mathrm{break}}$ as a function of the position of the tip with respect to the nanobridge. The directions x and y are defined in the inset.

tions, where x is parallel to the bridge and y is perpendicular. As expected, small displacements in y direction drastically reduce the sensitivity of the setup, i.e., a larger T_z is necessary for breaking the bridge. When exceeding a deformation in z direction of 30–45 μm (depending on the shape of the tip), the membranes break along the crystallographic [011] and [01−1] directions.

At variance to break junctions on bulk substrates which can be regarded as a homogeneous bending beam,[2] here the local elastic stretching of the membrane controls the deformation of the metal bridge. In order to control the elongation of the MCB, we need to estimate the strain of the membrane parallel to the leads at the location of the nanobridge. For that purpose we choose the following coordinate systems [see Fig. 6(a)]: The location (r_x, r_y) is measured relative to the tip and the tip position (T_x, T_y, T_z) relative to the center of the flat membrane. In general, the local strain ε depends on the location (r_x, r_y) and on (T_x, T_y, T_z). We assume here that the break junction is located in the center of a quadratic membrane with the edge length of d. Below we will focus on the case when the tip is positioned directly underneath the leads, that is, $T_y = 0$ and on locations on the leads, that is, $r_y = 0$. In the next step we assume that when the tip is near the center of the membrane, we can write the local strain ε as a product of the strain averaged over the entire lead and a symmetric weight function $e(r_x)$ that only depends on r_x,

$$\varepsilon(r_x, T_z, T_x) = e(r_x) \cdot \bar{\varepsilon}(T_z, T_x). \tag{1}$$

The definition of the average strain $\bar{\varepsilon}(T_z, T_x) = \int_{-d/2}^{d/2} dr_x \varepsilon(r_x, T_z, T_x)$ together with Eq. (1) leads to the standardization of the weight function,

$$\int_0^{d/2} dr_x e(r_x) = \frac{d}{2}. \tag{2}$$

On the other hand $\bar{\varepsilon}$ can easily be obtained by geometrical considerations [Fig. 6(a)],

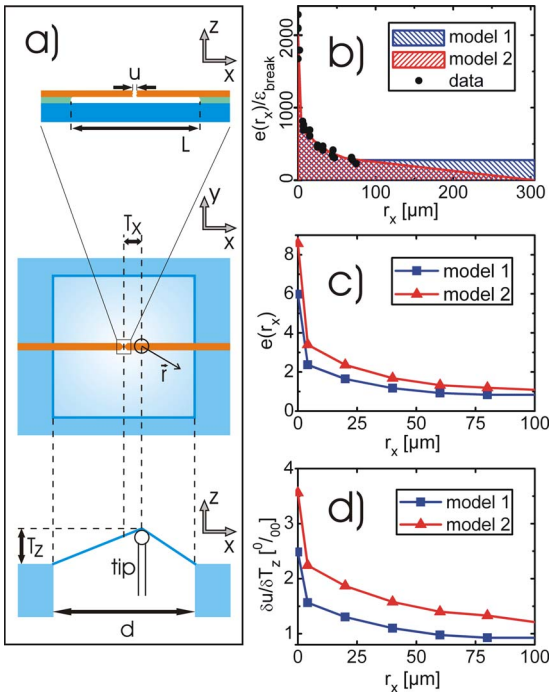

FIG. 6. (Color online) Schemes and data necessary for determining the relationship between the motion and the position of the tip and the resulting deformation of the membrane. (a) Scheme of the sample geometry (not to scale) with all relevant dimensions (see text). (b) Relative elongation $e(r_x)/\varepsilon_{\text{break}}$ of the membrane. The data points have been calculated with Eq. (5) and the data in Fig. 5. The lines are two different extrapolations of the data, which we name models 1 and 2. (c) Weight function $e(r_x)$ deduced from models 1 and 2. (d) Relative motion $\delta u/\delta T_z$ as a function of the tip position along the x axis for models 1 and 2 (for details, see text).

$$\bar{\varepsilon}(T_z,T_x)=\frac{\sqrt{\left(\frac{d}{2}+T_x\right)^2+T_z^2}+\sqrt{\left(\frac{d}{2}-T_x\right)^2+T_z^2}}{d}-1. \tag{3}$$

In Fig. 5 we depict the tip positions in z direction $T_{z,\text{break}}$ where the MCB breaks for a given tip location in the membrane plane. We assume that the relevant point for the local strain is the center of the membrane (where the nanobridge is located): $r_x=-T_x$. Since the contact always breaks under the same strain $\varepsilon_{\text{break}}$, we can conclude,

$$\varepsilon(r_x=-T_x,T_{z,\text{break}},T_x)=\varepsilon_{\text{break}}=\text{const.}, \tag{4}$$

and with Eq. (1) and the symmetry of $e(r_x)$ it follows

$$\frac{e(r_x=T_x)}{\varepsilon_{\text{break}}}=\frac{1}{\bar{\varepsilon}[T_{z,\text{break}}(T_x),T_x]}. \tag{5}$$

On the right hand side we insert the empirical data from Fig. 5 and the expression Eq. (3) to gain $e(r_x)/\varepsilon_{\text{break}}$ [see Fig. 6(b)]. An estimated value for the missing constant $\varepsilon_{\text{break}}$ can be obtained by the standardization condition Eq. (2): $\int_0^{d/2}dr_x e(r_x)/\varepsilon_{\text{break}}=d/2\varepsilon_{\text{break}}$.

The integral depends on the extrapolation of the experimental data to the border of the membrane. We are confident that the true value is somewhere between models 1 and 2 defined in Fig. 6(b) leading to $\varepsilon_{\text{break}}$ between 0.30% and 0.43% for this sample.

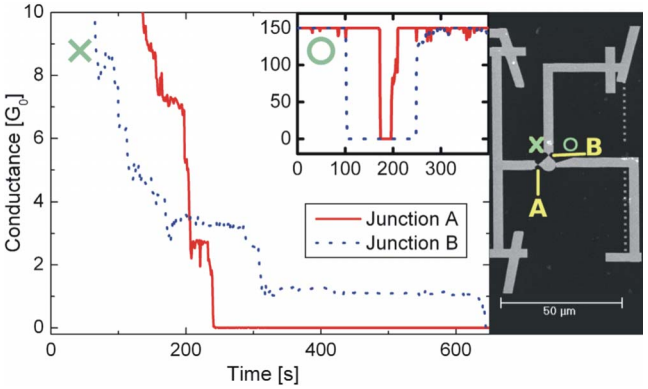

FIG. 7. (Color online) Conductance vs time of junctions A and B of the circuit shown in the right panel when the tip was located at the position indicated by the cross. Inset: Conductance vs time of junctions A and B of the circuit shown in the right panel when the tip was located at the position indicated by the circle. At $t=160$ s the motion direction of the tip is reversed. Right panel: The cross (circle) indicates the tip positions at which the opening curves shown in the left panel and the inset have been recorded.

Now we have the weight function $e(r_x)$ [Fig. 6(c)], and with it the local strain ε responsible for the breaking of the MCB allowing us to calculate the reduction ratio

$$\rho=\frac{\delta u}{\delta T_z}=L\frac{\partial}{\partial T_z}\varepsilon \tag{6}$$

[see Fig. 6(d)]. The lower the reduction ratio, the easier it is to maintain stable contacts over a long period of time. For the standard MCB on a massive substrate, ρ is a constant for a given sample layout. On membranes, we have to be more specific since ρ depends on the same parameters as the local strain. To make things easier it can be shown that for the relevant range of parameters, i.e., $T_z<35$ μm and $|T_x|<50$ μm, the following term is a good approximation of Eq. (3):

$$\bar{\varepsilon}=2\frac{T_z^2}{d^2}. \tag{7}$$

For the issue of stability we are interested in ρ at the point of breaking, $\rho_{\text{break}}=(\delta u/\delta T_z)|_{T_z=T_{z,\text{break}}}=L\,(\partial/\partial T_z)\varepsilon(r_x=-T_x,T_z,T_x)|_{T_z=T_{z,\text{break}}}$ using Eqs. (1), (4), and (7) we obtain an expression that can be calculated using the empirical data for $\varepsilon_{\text{break}}$ and $e(x)$ [see Fig. 6(c)]: $\rho_{\text{break}}=(2\sqrt{2}L/d)\sqrt{e(T_x)\varepsilon_{\text{break}}}$. Empirically we find $\rho\approx 0.001$ when the tip is located underneath the bridge. Detailed observation of the shape of the membrane reveals that the elastic limit of the membrane is higher than the one of the metal film. This study will be published elsewhere.

B. Control of multijunction devices

The versatility of the technique is demonstrated by controlling two junctions which are arranged perpendicularly to each other [see Fig. 1(b)]. Figure 7 shows the conductance of both junctions as a function of time when opening and closing with constant speed for different positions in the x-y plane. When positioning the tip close to junction A, junction B is mainly unaffected and vice versa. In this particular experiment it was our goal to find the position at which both

junctions have comparable size in the few-atom regime, with similar conductance values and break at a similar T_z. This would, for example, be required for studying charging effects in metallic single-electron transistors with variable junctions. As can be seen from Fig. 7 for this sample layout the desired situation was approximately obtained for the tip position indicated by a cross in the right panel of Fig. 7. The inset of Fig. 7 shows an example in which junction B opens and closes well before a conductance change can be recorded for junction A (tip located at the circle in the right panel of Fig. 7).

C. Influence of light irradiation onto the conductance of atomic-sized contacts

When irradiating break junctions with laser light, many effects may occur, including — among others — thermal expansion of the metal and the substrate, the excitation of photocurrents, or conductance changes, due to the excitation of hot electrons.[12,13] For studying the effect of electronic excitations thermal expansion and other influences of the substrate should be reduced as much as possible. For this goal our new technique is advantageous as well: The thin silicon membranes are almost transparent for visible light and the thermal contact between metal and membrane is much better because of the smaller thickness of the polyimide layer. In Fig. 4(b) we plot the conductance of a gold junction when driving the tip with constant z-speed as a function of time when irradiating with laser light with a wavelength $\lambda=488$ nm and varying power P as indicated in the legend. We observe an enhancement of the conductance which is roughly proportional to P for almost all values of G. The size of the conductance change varies remarkably from plateau to plateau although they may have very similar conductance. An example for this observation is given for the two adjacent plateaus for $G\approx 2.5G_0$ with a conductance changes $\Delta G_1=0.2G_0$ and $\Delta G_2=0.05G_0$. From this observation we deduce that the conductance changes depend on the individual atomic arrangement of the contacts, which rules out thermal expansion effects of the substrate or the metallic electrodes.

V. CONCLUSIONS

In conclusion, we have introduced a new variation of MCBs, which are realized on thin silicon membranes. We demonstrated the stability of the technique which is sufficient to stabilize and to characterize the transport properties of single-atom contacts under the influence of external control parameters. The technique overcomes the limitation of the existing MCB experiments because it allows us to control more than one junction on the same circuit. We will use it for studying the influence of optical excitations onto the conductance[12,13] and for controllable metallic single-electron transistors.[14]

ACKNOWLEDGMENTS

We are indebted to T. Dekorsy, A. Erbe, and P. Leiderer for fruitful discussions. We thank G. Hahn (Photovoltaics group) for use of equipment and F. Book, H. Haverkamp, and A. Herguth for their contributions to the membrane preparation. We gratefully acknowledge financial support from the DFG through SFB767.

R.W. and O.S. contributed equally in this work.

[1] N. Agraït, A. Levy Yeyati, and J. M. van Ruitenbeek, Phys. Rep. **377**, 81 (2003).
[2] C. J. Muller, J. M. van Ruitenbeek, and L. J. de Jongh, Physica C **191**, 485 (1992).
[3] J. M. van Ruitenbeek, A. Alvarez, I. Piñeyro, C. Grahmann, P. Joyez, M. H. Devoret, D. Esteve, and C. Urbina, Rev. Sci. Instrum. **67**, 108 (1996).
[4] M. Bruel, Electron. Lett. **31**, 1201 (1995).
[5] J. M. van Ruitenbeek, E. Scheer, and H. Weber, in *Introducing Molecular Electronics*, Lecture Notes in Physics, edited by G. Cuniberti, G. Fagas, and K. Richter (Springer, New York, 2005).
[6] P. Leiderer, C. Bartels, J. König-Birk, M. Mosbacher, and J. Boneberg, Appl. Phys. Lett. **85**, 5370 (2004).
[7] K. Ueno, S. Juodkazis, V. Mizeikis, K. Sasaki, and H. Misawa, Adv. Mater. (Weinheim, Ger.) **20**, 26 (2008).
[8] J. J. Parks, A. R. Champagne, G. R. Hutchison, S. Flores-Torres, H. D. Abruña, and D. C. Ralph, Phys. Rev. Lett. **99**, 026601 (2007).
[9] J. Butschke, A. Ehrmann, E. Haugeneder, M. Irmscher, R. Kaesmaier, K. Kragler, F. Letzkus, H. Loeschner, J. Mathuni, I. W. Rangelow, C. Reuter, F. Shi, and R. Springer, Proc. SPIE **3665**, 20 (1999).
[10] C. M. Sotomayor Torres, A. Zwick, F. Poinsotte, J. Groenen, M. Prunnila, J. Ahopelto, A. Mlayah, and V. Paillard, Phys. Status Solidi C **1**, 2609 (2004).
[11] A. Degen, N. Abedinova, T. Gotszalkb, E. Sossnaa, M. Kratzenberga, and I. W. Rangelow, Microelectron. Eng. **57**, 425 (2001).
[12] J. K. Viljas and J. C. Cuevas, Phys. Rev. B **75**, 075406 (2007).
[13] D. C. Guhr, D. Rettinger, J. Boneberg, A. Erbe, P. Leiderer, and E. Scheer, Phys. Rev. Lett. **99**, 086801 (2007).
[14] H. Grabert and M. H. Devoret, *Single Charge Tunneling*, NATO ASI Series Vol. 294 (Plenum, New York, 1992).